Effects of network morphology on the failure stress of highly porous media

Chung, J.W; de Hosson, J.T.M.

Published in:
Physical Review B

DOI:
10.1103/PhysRevB.66.064206

Publication date:
2002

Effects of network morphology on the failure stress of highly porous media

J. W. Chung and J. Th. M. De Hosson*
Department of Applied Physics, Materials Science Centre and Netherlands Institute of Metals Research, University of Groningen, Nijenborgh 4, 9747 AG Groningen, The Netherlands

(Received 3 October 2001; revised manuscript received 11 April 2002; published 15 August 2002)

In this study four types of morphologies are generated to illustrate the importance of the details of the network structure in relation to its mechanical strength while keeping the density fixed. By varying the disorder parameter in a dynamical system of weakly interacting void-volume spheres, it is possible to generate various correlated node distributions. A network of springs is constructed from the correlated node distribution, which can be sued to examine the failure characteristics of materials that are not governed by systems commonly derived from regular spring networks. The structures of the various morphologies are characterized by the normalized radial distribution of the nodes. Within a single phase the correlation length is the predominant parameter that determines the failure stress of the network.

DOI: 10.1103/PhysRevB.66.064206 PACS number(s): 46.50.+a

I. INTRODUCTION

Elastic networks of springs or beams are frequently used to model the relation between mechanical properties of materials and their microstructure.[1] Simulations have been carried out both in two and three dimensions,[2–8] mainly on regular spring network. The common way to construct a network is to use a regular node distribution and before the nodes are connected a preset fraction of the nodes is randomly removed. To introduce heterogeneity a random node displacement or bond strength distributions is used.[9,10] With the common use of random number generators, there is no correlation in the successive position of nodes. In contrast, in this work all node distributions are generated by a dynamical method[2] instead of using predefined correlated distributions or predefined node-node position rules.

In particular, this study is motivated by developments in the field of highly porous ceramic materials. The details of the microstructure prove to be as vital for the overall material strength as their porosity.[11] Moreover, the property that the mean void size can be changed without altering the empty volume is used in the manufacturing process of highly porous extrudates.[12,13] In practice, tailoring the interaction parameters of the emulsion particles alters the microstructure. Figure 1 shows scanning electron micrographs of two highly porous ceramics with different strength and different correlation length but having the same global porosity. The pore diameter and density were determined with mercury porosimetry as well as high resolution scanning and transmission electron microscopy. The density of silica depicted in Figs. 1(a) and 1(b) were found to be 0.7×10^3 kg m^{-3} and the corresponding strengths were 4.5 and 2.5 MPa, respectively. With a skeleton density of amorphous silica of approximately 2.2×10^3 kg m^{-3}, this leads for both systems to a volume porosity of 68% whereas the mechanical strength differ almost a factor of 2.

In this work a generation model for node distributions is used, which incorporates particle interactions. A disorder parameter T^* is employed to alter the entropy of the dynamical particle system. At various values of the disorder parameter node distributions are generated. These node distributions thus obtained are then converted into elastic spring networks by connecting every node with a spring if their relative distance is below a certain C_t, the so-called connectivity threshold. Each value of T^* yields spring networks of a different morphology. Next to the ball- and-stick visualizations of the different morphology, the normalized radial distribution function and density-density autocorrelation functions are presented. Failure of the networks under compression provides the possibility to relate the microstructure to the mechanical strength of the network.

II. COMPUTATIONAL PROCEDURE

Generation of network

The computational procedure starts with the generation of a node distribution. The molecular dynamics based algorithm uses N void volume spheres, which all have a Lennard-Jones interacting outer surface. The method provides a convenient way of generating a distribution of disordered nodes. The disorder is controlled by the preset values of the temperature and pressure thermostat.[14] The radii of the void volume spheres are taken to be 25 nm, and the Lennard-Jones[15] outer surface interaction, σ_{LJ}, is also set to 25 nm. The temperature of the reference bath is T^*, in units of ε/k_B where ε is the energy and k_B is Boltzmann's constant. The pressure reference bath P^0 is preset to a value of $0.4\varepsilon/\sigma_{\mathrm{LJ}}^3$. Those values are found to be sufficient to generate a disordered spatial distribution[16] of particles. The T^* values of the reference bath used were 0.0, 0.5, 1.0, 1.5, 2.0, 2.5, 3.0, 5.0, 8.0, and 14.0. As a reference one can notice that the Lennard-Jones triple point is produced with a void volume equals 0.0, a T^* set equal to 0.78, and P^0 equals 1.275.

The relaxation process took 25 000 time steps in order to attain equilibrium using a time increment step Δt of 10^{-9} s. The leapfrog integration scheme[17] calculates the position and velocities of the particles using the Newtonian equations of

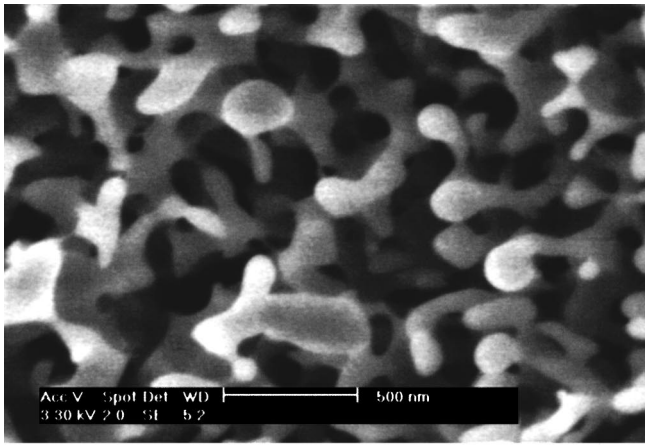

(a)

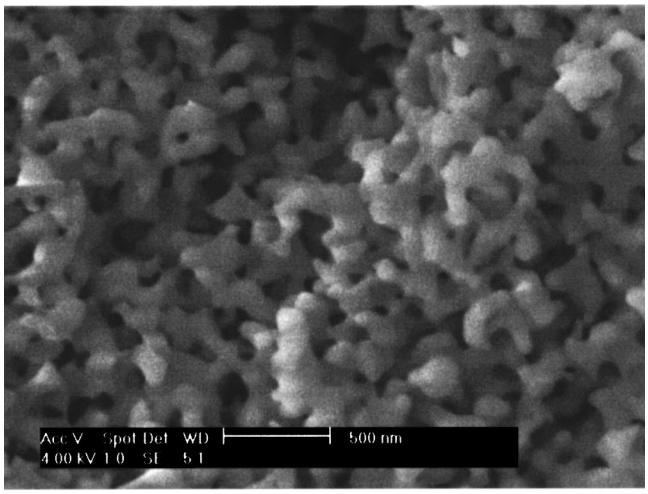

(b)

FIG. 1. Two scanning electron micrographs (SEM's) of highly porous ceramics with different strength and different correlation length having the same porosity (68%). (a) strength 4.5 MPa. (b) 2.5 MPa.

motion. The driving force for each particle in each step is the superposition of all the interactions of the particle with its neighboring particles. After the first 20 000 time steps nine node distributions are sampled. All the distributions are taken with 2000 consecutive time steps in between.

The thermostat maintains a constant pressure in the mesoscopic particle system. This is achieved by adjusting the box size. To remove the effect of the node density all the node distributions are scaled to an average node density of 500 nodes/μm^3, resulting in a fixed box size of $1.0\times1.0\times2.0$ μm^3.

The generated distributions form the basis of the spring connecting procedure. Every node is a potential point of connection, and as a consequence the geometry of the network is globally fixed by the positions of the nodes. Actually, only the interaction length between the nodes is left as a parameter. The node interaction between two nodes exists only if their relative distance is below the connectivity threshold C_t. Depending on the value of C_t, the system may develop from fully connected, i.e., every node is connected with all the other nodes, to a lowest finite value where all nodes are still connected. Roughly speaking, for low C_t and low disorder the network resembles the Delaunay network, whereas for higher C_t values the network geometry will deviate more and more from it. In this investigation C_t is 0.15 μm. This value is one of the lowest C_t values that could be addressed, while remaining a network with a constant average node density.

TABLE I. The disorder parameter T^* (units of ε/k_B) and the resulting phase.

Disorder parameter $T^*(\varepsilon/k_B)$	Phase	Examples
0.0	Regular grid (simple cubic)	
0.25, 0.5, 1.0, 1.5, 2.0	Structured	Figures 3 and 4
2.5, 3.0	Condensed	Figure 5
5.0, 8.0, 16.0	Random	Figure 6

The structure is represented by ball- and-stick visualizations, the normalized radial distribution functions and density-density autocorrelation functions. The radial distribution function (RDF), is calculated from $4\pi r^2 g(r)$ where the pair distribution $g(r)$ is given by:

$$\rho_0 g(\mathbf{r}) = \frac{1}{N}\sum_i^N \sum_j^N \delta[\mathbf{r}-\mathbf{R}_{ij}] - \delta(\mathbf{r}). \tag{2.1}$$

N represents the total number of spheres, $\rho_0 (=N/V)$ is the number density, and $\mathbf{R}_{ij}$ is the vector between centers of particles i and j. The normalization of the radial distribution function is obtained by integrating over all possible separations of the two spheres in Eq. (2.1).

The density-density autocorrelation function is calculated from[18]

$$\Gamma(\mathbf{r}) = \frac{\int \rho(\mathbf{r}'+\mathbf{r})\rho(\mathbf{r}')d\mathbf{r}'}{\int |\rho(\mathbf{r})|^2 d\mathbf{r}}, \tag{2.2}$$

where the density distribution function $\rho(\mathbf{r}) = \rho_0 g(\mathbf{r})$ presents the radial density function at point $\mathbf{r}$. Generally speaking, we may envisage $\Gamma(\mathbf{r})$ as a decreasing function of $\mathbf{r}$ with the limits, $\Gamma(\mathbf{r})\to 1$ as $\mathbf{r}\to\mathbf{0}$ and $\Gamma(\mathbf{r})\to 0$ as $\mathbf{r}\to\infty$. The density-density autocorrelation falls off rapidly at distances

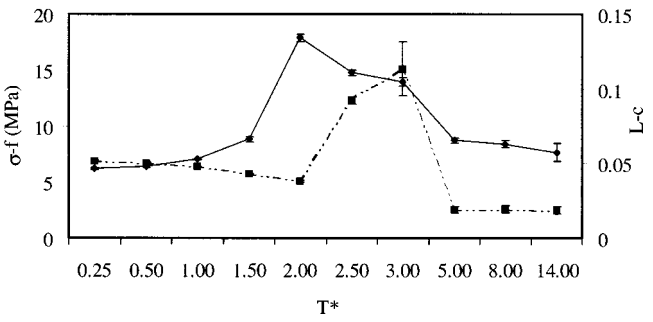

FIG. 2. The failure stress σ_F (◆, MPa left axis) and the correlation length L_c (■, units 1 μm, right axis) vs the disorder parameter T^*.

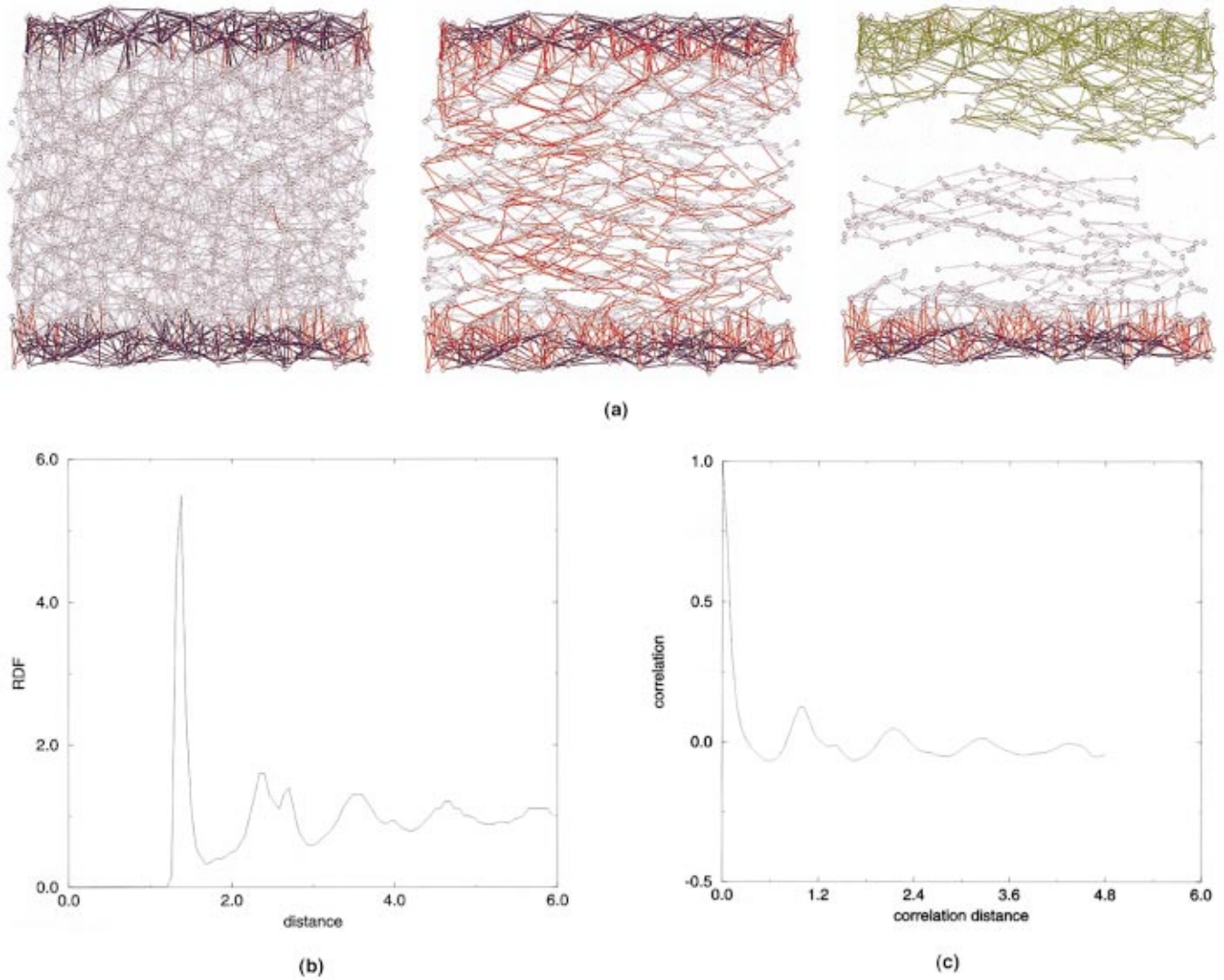

FIG. 3. (Color) (a) Three phases of the fracture process (start, intermediate, and final stages, respectively) in the structured phase ($T^*=0.25$). Blue bonds are connected to nodes in the top or bottom layers. Red bonds fulfil the fracture criterion. The network has fallen apart in two separated parts, one of which is colored green. (b) The normalized radial distribution function as a function of the distance ($T^*=0.25$, distance in units of 100 nm). (c) The density-density autocorrelation function as a function of the distance ($T^*=0.25$, distance in units of 100 nm).

greater than a so-called correlation length. Here we take the value of $\mathbf{r}$ for which $\Gamma(\mathbf{r})$ goes to zero for the first time as a measure of the range of order in the material L_c. The coordination number CN is taken as the number of connections for a particular chosen value of C_t, and can also be calculated from:

$$\mathrm{CN}^{(1)} = \int_{r_0}^{C_t} 4\pi r^2 g(r)\, dr \tag{2.3}$$

where r_0 is the left-hand edge of the first peak in the radial distribution function.

Compression of network of the spring network is carried out along the procedure that has been delineated extensively in Refs. 2, 16, and 19 and will not be repeated here. The spring networks are loaded in compression and after each force increment, the network configuration with the lowest energy is calculated. The total elastic energy is described by a two-body central force, a three-body bond bending, and a four-body torsion (T) contribution, all with an E modulus of 400 MPa. Nevertheless, it should be emphasized that the difference with the previous work is the way the network is initially created. In the present work the molecular dynamics code is used to fix the node positions before the spring network code is run. In this way, it is possible to create different network topologies by adjusting the ''node temperature.'' In fact, the numerical experiments seek to investigate how the failure strength changes as a function of the node temperature. In this way it leads to a convenient methodology to generate different distributions with the temperature as a single control parameter. Of course the molecular-dynamics code is only used for a convenient generation of the network, and as such there is no link to the physical formation of a ceramic material.

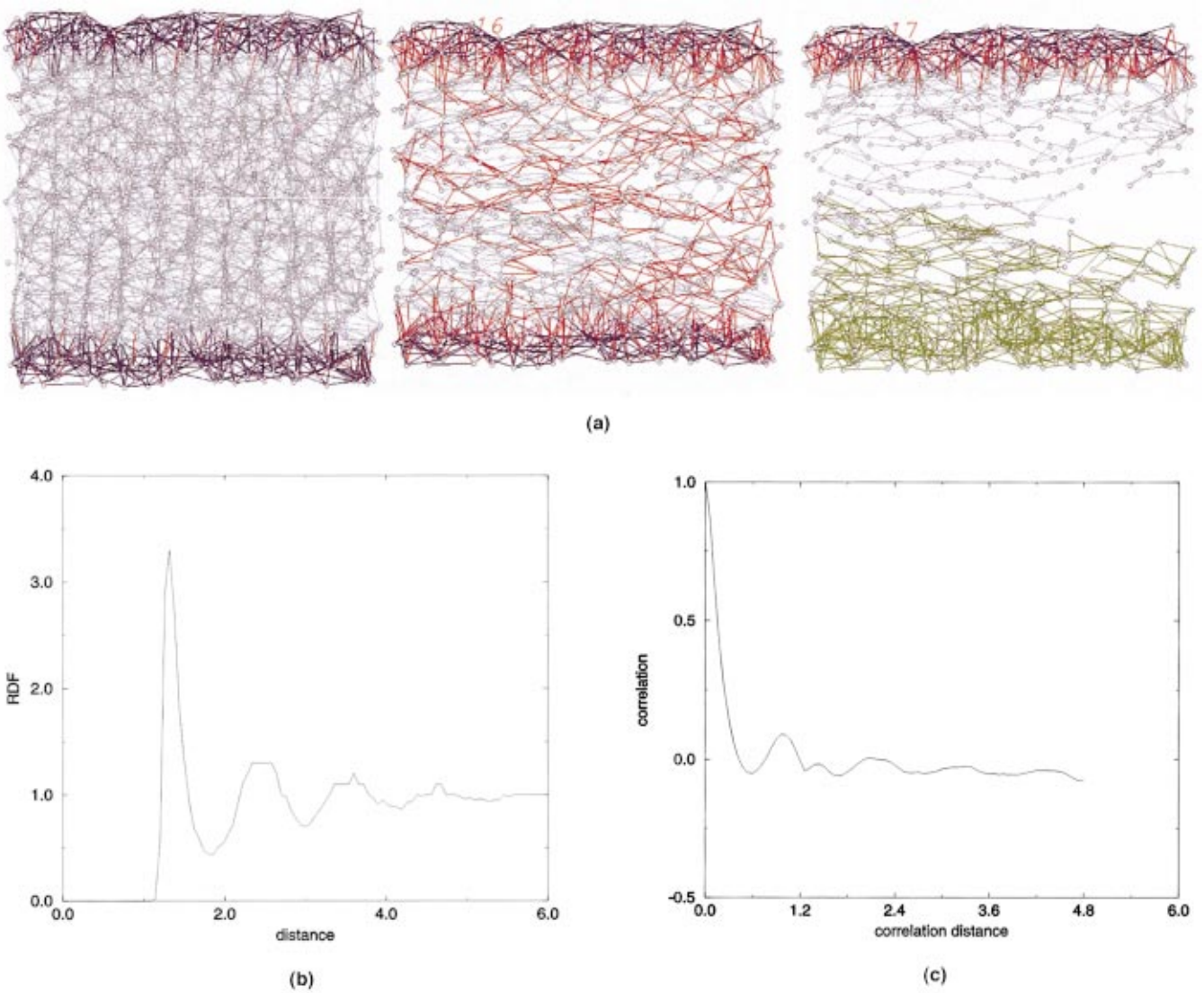

FIG. 4. (Color) (a) Three phases of the fracture process (start, intermediate, and final stages, respectively) in the structured phase ($T^*=1.5$) Blue bonds are connected to nodes in the top or bottom layers. Red bonds fulfil the fracture criterion. The network has fallen apart in two separated parts, one of which is colored green. (b) The normalized radial distribution function as a function of the distance ($T^*=1.5$, distance in units of 100 nm). (c) The density-density autocorrelation function as a function of the distance ($T^*=1.5$, distance in units of 100 nm).

The fracture criterion that is applied throughout this work is the maximum strain of 0.25%. The same value is also applied as fracture criterion for bond length and angular distortion. Once the fracture strain is satisfied in a spring element, the bond is removed from the network. Nodes without connection (floating nodes) or groups of unconnected nodes (fragments) are also removed from the interaction matrix. As a result of the removal of floating nodes and fragments, the possible effects of these fragments on the actual failure stress are explicitly ignored. An exception is maintained for the first layer on top and the last layer at the bottom of the sample with a thickness of 10 nm. All connections emerging from the nodes lying within these two layers are not subjected to fracture. This is done to take into account the fragmentation effect at the contact area. Actually, these unremoved nodes will effectively transmit the load similar to the ability of the fragments to transmit the load in real experiments.

III. RESULTS AND DISCUSSION

During the computer experiments several independent node distributions were generated for each of the disorder parameter values T^*. In Table I the disorder parameters values are listed. The parameter values are grouped according to the various phases. In the case of T^* equals 0, the resulting morphology is a regular grid (simple cubic structure). Figure 2 summarizes the results of the failure stress as a function of the disorder parameter T^*.

In the following figures all ball- and-stick visualizations are displayed in projection and the corresponding normalized radial distribution function are presented, together with the

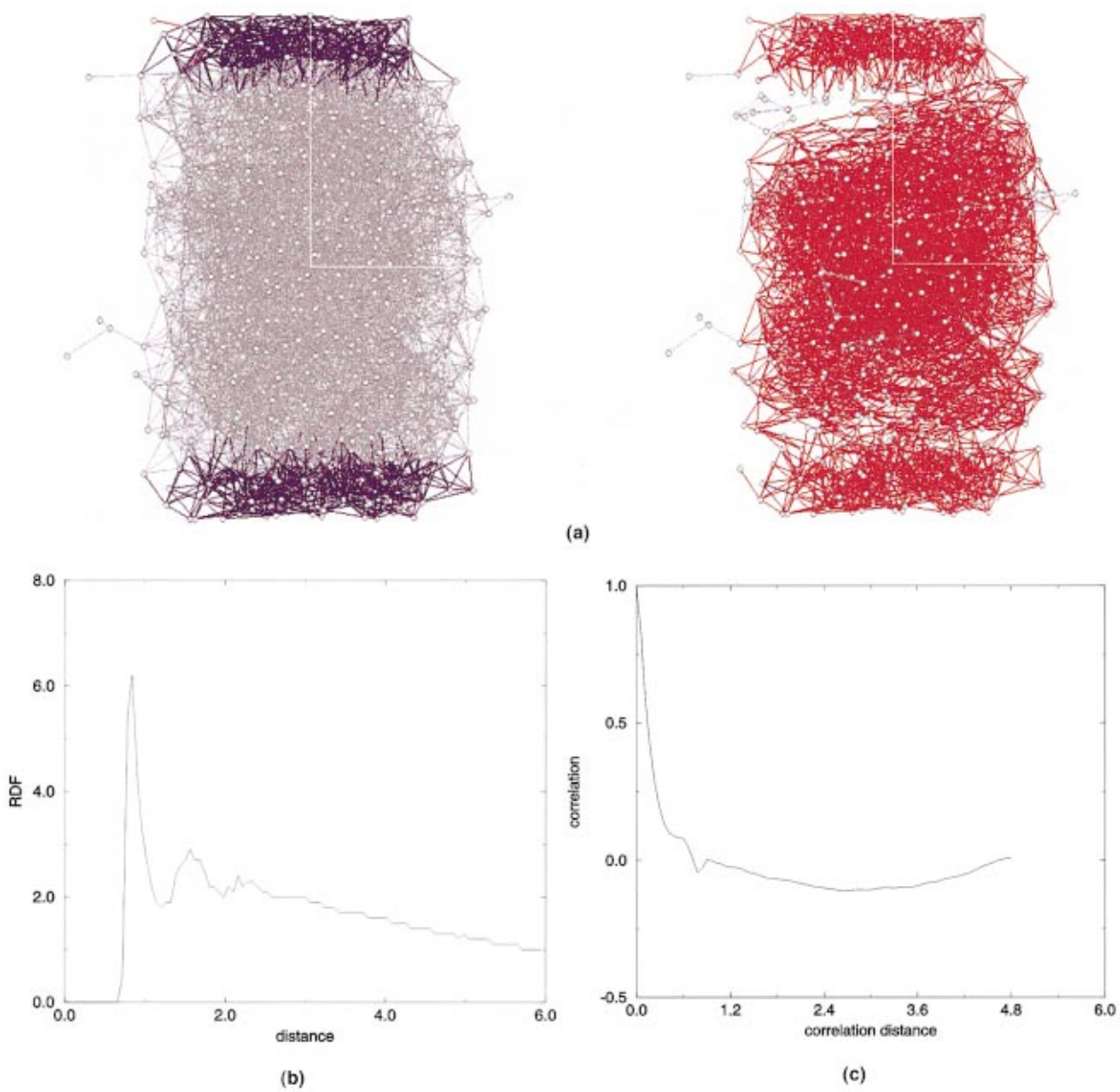

FIG. 5. (Color) (a) Two phases of the fracture process (start and final stages, respectively) in the condensed phase ($T^*=2.5$). Blue bonds are connected to nodes in the top or bottom layers. Red bonds fulfil the fracture criterion. (b) The normalized radial distribution function as a function of the distance ($T^*=2.5$, distance in units of 100 nm). (c) The density-density autocorrelation function as a function of the distance ($T^*=2.5$, distance in units of 100 nm).

density-density autocorrelation function. We have calculated nine node distributions for every particular T^* listed in Table I. However, the figures of normalized radial distribution functions and density-density autocorrelation functions are only for one node distribution per T^*.

Figures 3(a) and 4(a) show a node distribution with T^* in the range between 0.25 and 2.0. The corresponding normalized radial distribution functions and density-density autocorrelation functions are shown in Figs. 3(b), 4(b), and 3(c), 4(c), respectively. The node distribution is denoted as a so-called structured distribution. This can be easily recognized by the higher order peaks in the normalized radial distribution functions. The preset T^* values of 2.5 and 3.0 produce a condensed phase system. Figure 5 shows the configuration that belongs to T^* equals 2.5. The system consists of a highly netted part surrounded by an almost non-interacting part. Actually, the latter can be regarded as a gaseous phase. Because the nodes without interacting connections and also groups of unconnected nodes are removed these gaseous areas in Fig. 5(a) are empty. Throughout the calculation the same connection criterion is used and therefore one would expect that the condensed phase must be remarkable stronger that the structured phase. As depicted in Fig. 2, T^* equal to 2.0 seems to produce node distributions that are as strong as the distributions representing the condensed phase. Examples of a phase that belongs to an even higher T^*, namely, 8 and

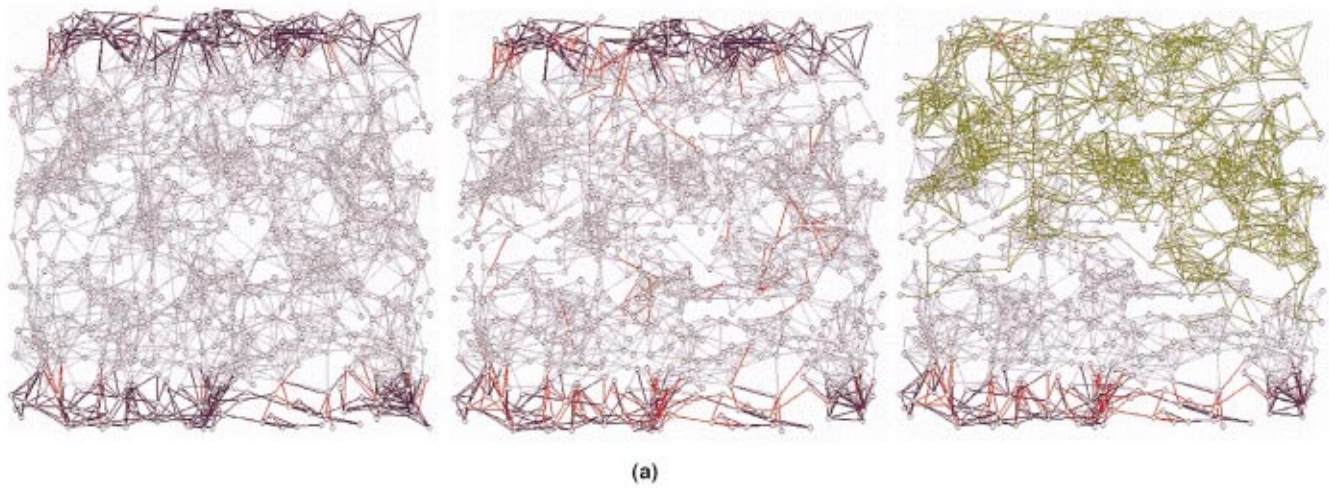

(a)

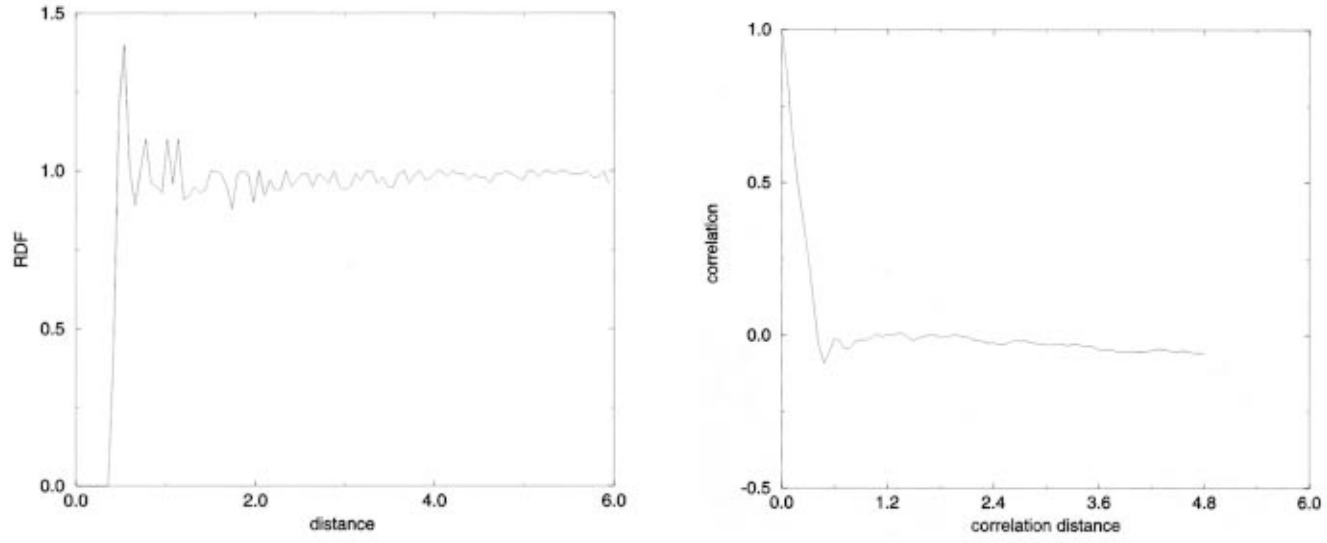

(b) (c)

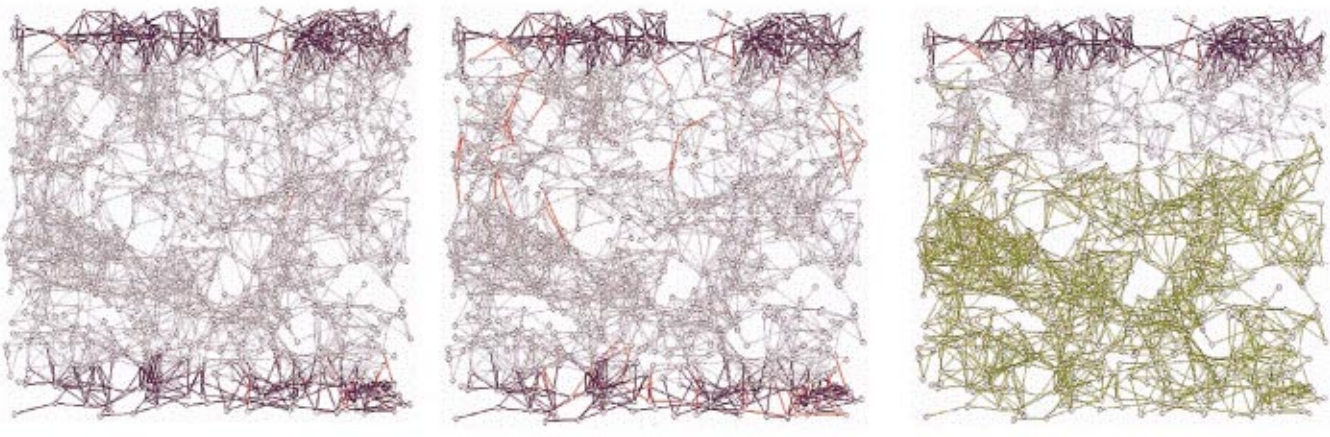

(d)

FIG. 6. (Color) (a) Three phases of the fracture process (start, intermediate, and final stages, respectively) in the random phase ($T^*=8$). Blue bonds are connected to nodes in the top or bottom layers. Red bonds fulfil the fracture criterion. The network has fallen apart in two separated parts, one of which is colored green. (b) The normalized radial distribution function as a function of the distance ($T^*=8$, distance in units of 100 nm). (c) The density-density autocorrelation function as a function of the distance ($T^*=8$). (d) Three phases of the fracture process (start, intermediate, and final stages respectively) in the random phase ($T^*=14$, distance in units of 100 nm). Blue bonds are connected to nodes in the top or bottom layers. Red bonds fulfill the fracture criterion. The network has fallen apart in two separated parts, one of which is colored green.

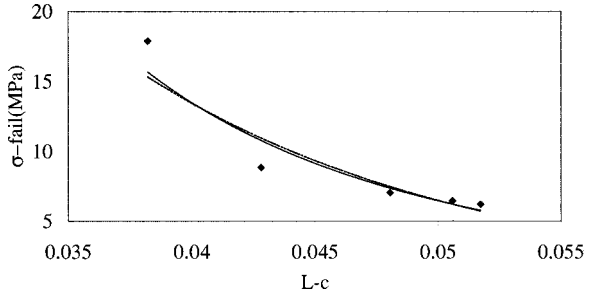

FIG. 7. Failure stress (MPa) vs correlation length L_c (units 1 μm) in the structured phase (solid line exponential decay, dashed line power-law behavior).

14, are displayed in Figs. 6(a) and 6(d), together with the corresponding normalized radial distribution function and density-density autocorrelation function for $T^*=8$ in Figs. 6(b) and 6(c) respectively. The phase in Fig. 6 is called the random phase. For T^* ranging between five and 14 random configurations are produced that contain large voids. The larger the T^* the larger the voids seems to be [see Figs. 6(a) and 6(d)]. Although a pronounced first peak is found, no distinct higher order peaks are detected in the normalized radial distribution, see Fig. 6(c). Actually, the first peak in the RDFs reveals a local clustering behavior and a mean distribution at longer distances.

Figure 7 shows the failure stress as a function of the range of order, the correlation length L_c. A significant increase in strength is observed with decreasing correlation length. L_c in the randomlike phase is slightly decreasing with increasing T^* and so is the failure stress. This is in contrast to the correlation between the failure stress and L_c for the structured phase. Here, the failure stress decreases, either exponentially or as a power law, with increasing L_c.

In this context it would be interesting whether we can cast the mechanical behavior in a universal type of description, such as

$$\sigma_c - \sigma \propto (\varepsilon_c - \varepsilon)^{1/\mu}, \tag{3.1}$$

where σ and ε are the global stress and strain, respectively and where the subscripts c denotes the peak values of these quantities. We have carried out this analysis for the structured phase ($T^*=0.25$) and random phase ($T^*=8$). The starting, intermediate and final configurations are depicted in Figs. 3(a) and 6(a), respectively. It turned out that in both cases σ could be described by $\alpha\varepsilon^{1/\beta}$, where the precise value of α and β depend on T^*, with β in the former case (1.2 for $T^*=0.25$) smaller than in the latter (2.2 for $T^*=8$). The analysis leads to an exponent μ, which is not constant, i.e., not universal, being smaller in the case of $T^*=0.25$ (namely, 0.6) than for $T^*=8$ (namely, 0.8). Both critical stress and strain depend on T^* and so does the exponent μ. It supports the idea that there doesn't exist a universality relationship like Eq. (3.1) but that the exponent depends sensitively on the detailed topology in these systems (also see Table II).

It can be concluded from this work that a disorder parameter T^* in the node distribution generation method can be used to generate a large variety of node distributions. In the figures shown, both the strength and microstructure of the networks differ but the node density remains the same. The paper shows that a dynamical method of generating various node distributions provides a mean to generate networks and corresponding strength that are not governed by the common construction of networks derived from a regular grid, even if those grid-based networks are transformed by random node annihilation. The dynamical method does not need predefined rules of a correlated node distribution.

TABLE II. Numerical results: disorder parameter $T^*(\varepsilon/k_B)$, failure stress σ_f (MPa), coordination number (CN), and autocorrelation length L_c (nm).

Phase	T^*	σ_f (MPa)	CN	L_c (nm)
Regular grid	0.0	1.8	2.7	0
Structured	0.25	6.2	4.3	52
	0.5	6.5	4.2	51
	1.0	7.1	4.0	48
	1.5	8.9	3.7	43
	2.0	17.9	3.5	38
Condensed	2.5	14.8	8.8	93
	3.0	13.9	9.0	113
Random	5.0	8.7	3.3	19
	8.0	8.4	3.3	19
	14.0	7.7	3.2	18

The basic elements of the generation method are to move void volume spheres with a weak interacting outer surface as the basic element in a periodic boundary box and the possibility to change the entropy by means of a disorder parameter. These simple properties in the node distribution method seem to be adequate to generate a correlated node distribution. The node distribution generation method produces results that are in a better agreement with the experimental observation of the strength of highly porous ceramics than the results obtained from random networks derived from a regular grid. The value of the failure stress lies in the same order of magnitude as in experiments.[11,20] In a highly correlated material like in the structured phase the introduction of more randomness enhances the materials strength. This effect is in accordance with experimental results that show that an increase in randomness contributes to a higher strength of ceramic materials. However, as can be concluded from the calculations: in a fully random phase an enhancement of the disorder diminishes somewhat the fracture strength. Using the model properties of the distribution generation method one can also state that an increase of disorder leads to dilution effect of the interacting void volume spheres. The importance of ordering on the network strength can also been derived from Fig. 2. Despite the fixed node density a variation in phase and correlation length cause a large difference in the failure stress.

It is interesting to note that very different structures with a constant node density can be obtained by changing T^* in a system of spherical void volume particles with a Lennard-Jones interacting outer surface. In this study different kinds of network morphologies are generated to illustrate the importance of the microstructure in relation with its strength

while keeping the density fixed. Within a particular phase the range of order, i.e., L_c, is the predominant factor characterizing the failure stress of the network. The microstructure and its phase can be adequately described by the density-density autocorrelation function. The correlation length reflects the range of order expressed by L_c. The work demonstrates the importance of the details of the node distributions on the failure strength. Although all the numerical simulations were done at the same node density and porosity different strength levels are achieved depending on the topology.

ACKNOWLEDGMENTS

The work described in this paper is part of the research program of the foundation for Fundamental Research on Matter (FOM Utrecht), and was supported by the Netherlands Organization for Scientific Research (NWO-The Hague). The authors are grateful to Dr. E. Botta and Dr. A. van der Ploeg for providing us the matrix solver, to J. Kraak (HPC computing center University of Groningen) for assistance in the computer visualization part, and to Professor E. van der Giessen for discussions.

*Corresponding author. Email address: hosson j@phys.rug.nl

[1] B. K. Chakrabarti and L. Gilels Benguigui, *Statistical Physics of Fracture and Breakdown in Disordered Systems* (Clarendon, Oxford, 1997).

[2] J. W. Chung, A. Roos, J. Th. M. De Hosson, and E. van der Giessen, Phys. Rev. B **54**, 15 094 (1996).

[3] I. C. van den Born, A. Santen, H. D. Hoekstra, and J. Th. M. De Hosson, Phys. Rev. B **43**, 3794 (1991); in *Fracture Processes in Concrete, Rock and Ceramics*, edited by J. J. M. van Mier, J. G. Rots, and A. Bakker (E & FN Spon, London, 1991), p. 231.

[4] S. Feng, P. N. Sen, B. I. Halperin, and C. J. Lobb, Phys. Rev. B **30**, 5386 (1984).

[5] H. J. Hermann, A. Hansen, and S. Roux, Phys. Rev. B **39**, 637 (1989).

[6] M. Sahimi and S. Arbabi, Phys. Rev. B **47**, 695 (1993).

[7] S. Arbabi and M. Hahimi, Phys. Rev. B **41**, 772 (1990).

[8] S. Arbabi and M. Hahimi, Phys. Rev. B **38**, 7173 (1988).

[9] S. Arbabi and M. Hahimi, Phys. Rev. Lett. **65**, 725 (1990).

[10] J. Wang, J. Phys. A **22**, L291 (1989).

[11] J. Aué and J. Th. M. De Hosson, Appl. Phys. Lett. **71**, 1347 (1997); J. Mater. Sci. **33**, 5455 (1998).

[12] A. Gervois and D. Bideau, in *Disorder and Granular Media*, edited by D. Bideau and A. Hansen (Elsevier, Amsterdam, 1997), pp. 1–34.

[13] Y. Kantor and I. Webman, Phys. Rev. Lett. **52**, 1891 (1984).

[14] H. J. C. Berendsen, J. P. M. Postma, W. F. van Gunsteren, A. DiNola, and J. R. Haak, J. Chem. Phys. **81**, 3684 (1984).

[15] M. P. Allen and D. J. Tildesley, *Computer Simulations of Liquids* (Oxford University Press, Oxford, 1992).

[16] J. W. Chung, J. Th. M. De Hosson, and E. van der Giessen, Phys. Rev. B **64**, 064202 (2001).

[17] R. W. Hockney, *Methods in Computer Physics* (Elsevier, Amsterdam, 1970), Vol. 9, p. 136.

[18] J. M. Ziman, *Models of Disorder* (Cambridge University Press, Cambridge, 1979), p. 26.

[19] J. W. Chung, J. Th. M. De Hosson, and E. van der Giessen, Phys. Rev. B **65**, 094104 (2002).

[20] D. Stauffer and A. Aharony, *Introduction to Percolation Theory*, 2nd ed. (Taylor & Francis, London, 1992).